Generation of hydroacoustic signals by oceanic subseafloor earthquakes: a mechanical model

A. Balanche C. Guennou J. Goslin C. Mazoyer, Abel Balanche, Claude Guennou, Jean Goslin, Camille Mazoyer

Geophys. J. Int. (2009) **177,** 476–480 doi: 10.1111/j.1365-246X.2009.04146.x

FAST TRACK PAPER

Generation of hydroacoustic signals by oceanic subseafloor earthquakes: a mechanical model

A. Balanche,[1] C. Guennou,[1] J. Goslin[1] and C. Mazoyer[2]

[1]*CNRS;* UMR 6538 *'Domaines Océaniques', Institut Universitaire Européen de la Mer, Université de Bretagne Occidentale, Université Européenne de Bretagne,* 29280 *Plouzané, France. E-mail: abel.balanche@univ-brest.fr*
[2]*Institut Universitaire Européen de la Mer, Université de Bretagne Occidentale, Université Européenne de Bretagne,* 29280 *Plouzané, France*

Accepted 2009 February 13. Received 2008 January 12; in original form 2008 October 14

SUMMARY

For more than 15 yr, the recording of hydroacoustic signals with hydrophones moored in a minimum sound-velocity channel, called the SOFAR (SOund Fixing And Ranging) channel, has allowed for detection and localization of many small-magnitude earthquakes in oceanic areas. However, the interpretation of these hydroacoustic signals fails to provide direct information on the magnitudes, focal mechanisms, or focal depths of the causative earthquakes. These limitations result, in part, from an incomplete understanding of the physics of the conversion, across the seafloor interface, from seismic waves generated by subseafloor earthquakes to hydroacoustic *T* waves. To try and overcome some of these limitations, we have developed a 2-D finite-element mechanical model of the conversion process. By computing an exact solution of the velocity field of the waterborne *T* waves, our model shows that a double-couple source mechanism of a subseafloor earthquake generates *T* waves, whose take-off angles are adequate to allow penetration into the SOFAR channel and efficient trapping by this waveguide. Furthermore, our model confirms that a double-couple source with a high *S*-wave content produces higher-amplitude *T* waves than a simple explosive source, which only generates *P* waves.

Key words: Seismic monitoring and test-ban treaty verification; Computational seismology, Mid-ocean ridge processes.

1 INTRODUCTION

Hydrophone arrays moored in the SOFAR channel, a low-velocity channel that acts as a waveguide for acoustic signals travelling in the ocean, have been used for more than 15 yr to detect and localize relatively low-magnitude (typically $M_w > 2.5$) subseafloor earthquakes (Fox *et al.* 2001; Dziak *et al.* 2004). The main reason for using hydrophone arrays is that the seismic waves are rapidly attenuated when they travel through the oceanic crust and upper mantle. This attenuation precludes land-based seismic networks from having detection and localization capabilities comparable to those of hydrophone arrays. Conversely, thanks to the low attenuation properties of the SOFAR channel, acoustic signals can be recorded at large epicentral distances and allow for acoustic monitoring of vast oceanic areas by hydrophones networks made up with a small number of instruments. For example, autonomous hydrophone arrays of four to six instruments deployed on the flanks of the Northern Mid-Atlantic Ridge (MAR) have succeeded in detecting and localizing 30–50 times more earthquakes along this slow-spreading ridge than did land-based networks during the same periods. Detection and localization of seismic events are made possible by picking arrival times of acoustic signals recorded by hydrophone arrays. These acoustic signals, termed '*T* waves', result from the conversion at the seafloor interface of seismic waves generated by subseafloor earthquakes. The space and time distribution of the seismicity, computed from the catalogues of events produced by interpreting hydrophone data, recorded during relevant multiyear periods of time, provide major insights into the accretion processs active along the axes of mid-oceanic ridges (e.g. Goslin *et al.* 2005) and into intraplate deformation phenomena (e.g. Fox & Dziak 1999).

However, more in-depth interpretations of the amplitudes and waveforms of *T* waves require a fuller understanding of the physics of the seismic to acoustic conversion mechanism at the seafloor interface and of the propagation of the *T* waves along the SOFAR channel. For example, empirical models are the only currently available means to link the acoustic source levels recorded by hydrophone arrays to the seismic size of the earthquakes (e.g. Dziak 2001). Several models have been proposed to explain the generation of *T* waves by subseafloor earthquakes. The first type of models (Johnson *et al.* 1963; Talandier & Okal 1998) invokes the conversion across a sloped seafloor, which produces *T* waves with adequate incidence angles, to become efficiently trapped within the SOFAR

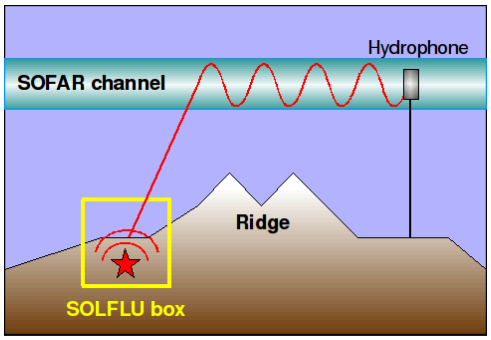

Figure 1. Cartoon showing the *T*-wave generation and propagation. The SOLFLU modelling is performed in the yellow box.

channel. This 'downslope propagation' model therefore requires a specific regional seafloor topography. However, *T* waves were later observed originating from events located in flat areas of the abyssal plains. This observation was termed the '*T*-phase paradox'. de Groot-Hedlin & Orcutt (1999) later proposed that local seafloor roughness in the vicinity of the epicentre would be responsible for the production of *T* waves. Their 'seafloor scattering model' produces two differents waves: a short onset-time, high-frequency 'abyssal *T*-phase', which would be generated by earthquakes located in deeper areas, and a 'slope *T*-phase', of lower frequency and shorter onset. However, a study by Williams *et al.* (2006), based on 158 events observed along the Mid-Atlantic Ridge, fails to confirm the relation between onset duration and seafloor depths at the conversion point as was proposed by de Groot-Hedlin & Orcutt (1999). Finally, a model based on the 'modal scattering' theory (Park *et al.* 2001) accounts for the generation of *T* waves by a rough seafloor in the epicentral region and provides first insight into the importance of the fault orientation in the *T*-wave excitation process.

The present work proposes a direct finite-element mechanical modelling of the conversion of seismic waves to acoustic waves at the seafloor interface (Fig. 1) to try and make some headway toward solving the *T*-phase paradox. Our model requires neither an *a priori* local topography nor a particular seafloor roughness. Our work addresses two main questions. First, how can *T* waves be generated at the seafloor with sufficient take-off angles to enter SOFAR channel? Second, what is the 'efficiency' of the seafloor conversion process for various types of seismic waves? In other words, how do the *P*- versus *S*-wave contents of various seismic sources influence the resulting *T*-wave signal characteristics?

2 MODEL DESCRIPTION

We have developed the 'solid to fluid' (SOLFLU) 2-D finite-element code to model the conversion of seismic–acoustic waves at the crust–water interface. The model presented here required major adaptations from a code developed for industrial applications involved in non-destructive testing control of cracks in complex structures (Bécache *et al.* 2001). This code was later adapted and applied to marine geophysical prospecting (Zhein *et al.* 2004). It should be noted that these two applications, which dealt with the conversion of acoustic wave propagating in a fluid to seismic waves in a solid medium, only allowed the implementation of a purely 'explosive' source producing only *P* waves, as *S* waves do not travel in the fluid source medium. Our new SOLFLU code allows the implementation of various types of sources located in the crust, such as double-couple source mechanisms, which generate crustal *P* and *S* waves both.

The SOLFLU code is based on the equations of continuum mechanics described below. Hooke's law (eq. 1) and the fundamental law of dynamics (eq. 2), which both relate stress to velocity are used to describe the propagation in the solid medium. The $\vec{v}_s$ and $\vec{v}_s$ velocity components are computed at the centre of each grid element. The stress tensor is computed at each grid node, where mass conservation equation (eq. 3) and Euler's law are used in the fluid medium. Similarly, the pressure is computed at the centre of each grid element and the velocity components at the centres of the sides of the grid elements (eqs 3 and 4). Eqs (5) and (6) model the boundary conditions at the solid/fluid interface. They express the continuity of the velocity component normal to the interface and the continuity of stress. To avoid reflection artefacts on the sides of the model box, propagating waves are absorbed by 'perfectly matched layers' (Collino & Tsogka 2001) whose thickness was chosen equal to 30 grid elements to have less than 0.01 per cent lateral reflection.

$$\overrightarrow{\overrightarrow{A}}\frac{\partial \overrightarrow{\overrightarrow{\sigma}}}{\partial t} - \overrightarrow{\overrightarrow{\epsilon}}\left(\mathbf{v_s}\right) = 0, \tag{1}$$

$$\rho_s \frac{\partial \mathbf{v_s}}{\partial t} + \nabla \overrightarrow{\overrightarrow{\sigma}} = 0, \tag{2}$$

$$\frac{\partial p}{\partial t} + c_f^2 \rho_f \nabla \mathbf{v_f} = 0, \tag{3}$$

$$\rho_f \frac{\partial \mathbf{v_f}}{\partial t} + \nabla p = 0, \tag{4}$$

$$\mathbf{v_s} \cdot \mathbf{n} = \mathbf{v_f} \cdot \mathbf{n}, \tag{5}$$

$$\overrightarrow{\overrightarrow{\sigma}} \cdot \mathbf{n} = -p(\overrightarrow{\overrightarrow{I}}) \cdot \mathbf{n}, \tag{6}$$

where $\overrightarrow{\overrightarrow{\sigma}}$ represents the stress, $\overrightarrow{\overrightarrow{\epsilon}}$ the time derivative of the strain tensor, $\overrightarrow{\overrightarrow{A}}$ the compliance tensor, $\overrightarrow{\overrightarrow{I}}$ the identity tensor, ρ_s and ρ_f the solid and fluid densities, $\mathbf{v}_\mathrm{s}$ and $\mathbf{v}_\mathrm{f}$ the solid and the fluid velocities, p the pressure within the fluid and $\mathbf{n}$ the unit normal vector.

3 MODEL INPUT

The physical parameters of both the solid and fluid domains and type of source are input into the model (see Table 1). A 10 × 10 km domain is described by a 1000 × 1000 grid of 10 × 10 m elements. For each case, the source is a Ricker pulse centred at 5 Hz and initial amplitudes for both compressive (*P* waves) and shear components (*S* waves) are normalized at the value one in the moment tensor source matrix. These parameters allow the modelling of the seismic to acoustic conversion with realistic space- and timescales.

Table 1. Model parameters for the 3 s runs.

Parameters	Values
Domain dimension (m)	10 000 × 10 000
Water colum depth (m)	3000
ρ_f(kg m^{-3})	1000
c_f(m s^{-1})	1500
ρ_s(kg m^{-3})	2900
cp_s(m s^{-1})	5500
cs_s(m s^{-1})	3175
Ricker source (Hz)	5
Source position (x,z)(m)	(5000, 8000)

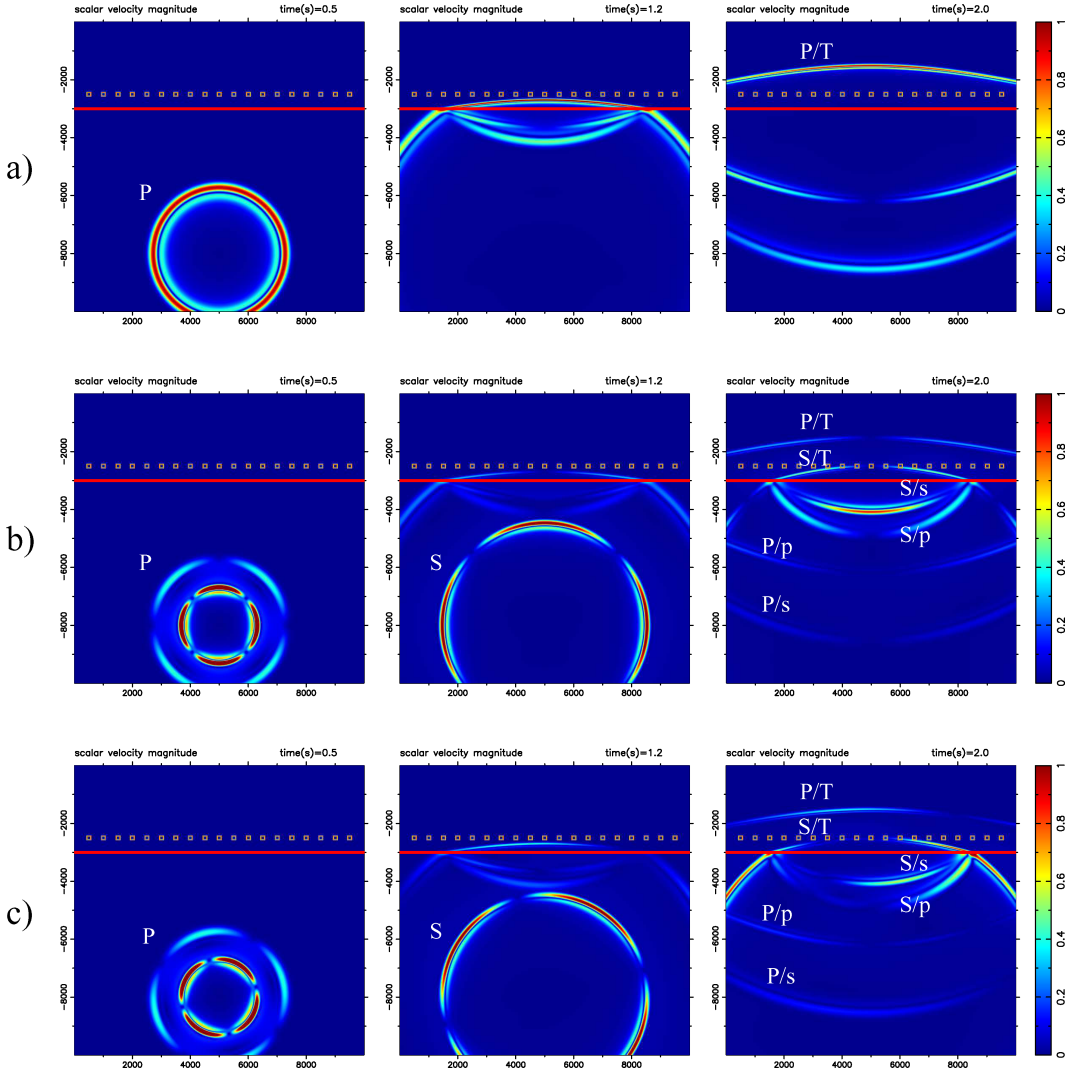

Figure 2. Snaphots of the scalar velocity magnitude of the wavefield modelled at 0.5, 1.2 and 2.0 s after the start of three 3 s runs. The horizontal line is the interface between the underlying solid crust and the overlying fluid. Squares show the positions of the 'synthetic sensors' placed 500 m above the interface. Distances along the X and Y-axis are in metres. The scale of the scalar velocity magnitude is arbitrary. P and S are the direct waves out of the source; P/p is, for example, the P wave reflected downward from the incident P wave at the solid/fluid interface; P/T and S/T are the converted T waves travelling in the fluid. From top to bottom: (a) the source is purely explosive; (b) the source is an horizontal double-couple mechanism; (c) the source is a slanted double-couple.

4 MODEL RESULTS

The results of three 3 s runs of the SOLFLU model are presented below. These model runs differ only by the type of source mechanisms, which were input into the model. Figs 2(a)–(c) show velocity snapshots at various times ($t_1 = 0.5$ s, $t_2 = 1.2$ s, $t_3 = 2.0$ s) for each of the three model runs.

The first run (Fig. 2a) begins with a purely 'explosive' source in the crust, 5 km below the seafloor. This source only generates isotropic P waves, which will later be converted to T waves. The second run (Fig. 2b) displays the propagation of the crustal and waterborne waves produced by a pure horizontal double-couple seismic source. This source generates both P- and S- seismic waves in the crust, which are in turn converted to P-to-T and S-to-T acoustic waves in the water column, respectively, noted P/T and S/T below. Note that this second runs produces multiple wave fronts, rather than the single wave front of the first model run. Finally, as the radiation pattern evidently depends on the fault plane orientation, a slanted double-couple mechanism representing the projection on a vertical plane passing through the hypocentre of the propagation of the waves generated by a normal fault event, is shown on Fig. 2(c). Various phases appear on the snaphots of Fig. 2(a) (explosive source case): in the solid, the direct P wave (P), the (P/p) and the (P/s) waves reflected downwards by the seafloor interface and in the fluid, the (P/T) converted T-phase. In the case of a double-couple source, additional phases are produced and are shown on Figs 2(b) and (c): the direct S wave travelling in the crust; the S/p and S/s waves, downward-reflected on the interface and, finally, the converted S/T contribution to the T waves. The snapshots shown on Figs 2(a)–(c) show that SOLFLU successfully models the major contribution of the S-wave component in the production of waterborne T waves.

To appreciate more precisely the amplitudes of the various waterborne phases during the model runs, a horizontal line of 'synthetic sensors' was positioned in the fluid, 500 m above the seafloor. Time-series of the $\mathbf{v}_{fx}$ and $\mathbf{v}_{fz}$ components of the deplacement velocity element were computed at each sensor. The maximum of the

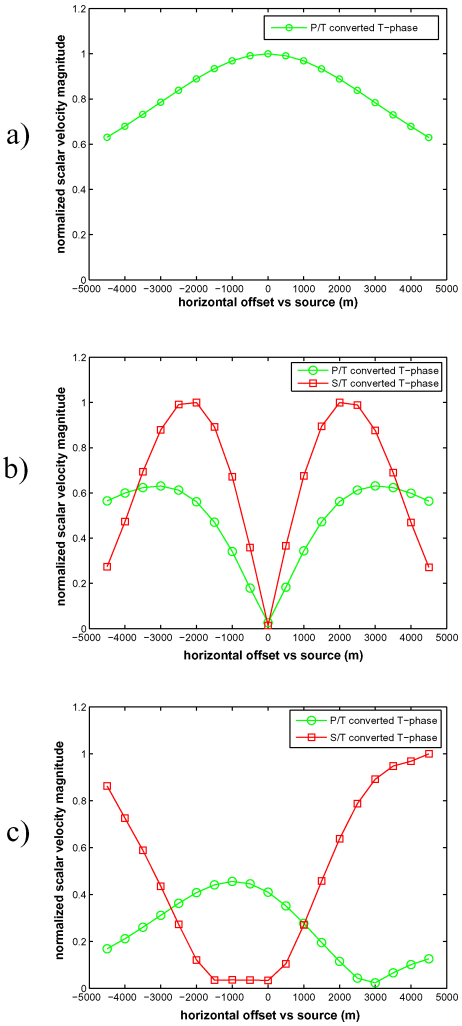

Figure 3. Normalized maxima of the scalar velocity magnitude versus horizontal offset along the line of 'synthetic sensors' (see positions of the sensors on Fig. 2). Source characteristics are as Fig. 2, that is, from top to bottom: (a) explosive; (b) horizontal double-couple; (c) slanted double-couple.

scalar velocity magnitude at each sensor, that is, max $(\sqrt{v_{fx}^2 + v_{fz}^2})$, was finally extracted from these time-series. These maxima were, in turn, normalized to the higher value for each source type and displayed on Fig. 3 below.

The maximum scalar velocity magnitude is proportional to the pressure (eq. 4 above) and can therefore be linked to the source level (SL) of earthquakes computed from the acoustic signals recorded by hydrophones moored in the SOFAR channel (for a definition of SL, see, e.g. Dziak 2001). Figs 3(a)–(c) further illustrate the differences between the two types of sources. In the case of the purely explosive source (Fig. 3a), the maximum of the converted wave pressure is observed near the vertical. It will thus enter the SOFAR channel at a low incidence angle and will not be efficiently trapped inside the waveguide. In the case of the double-couple mechanism, the 'sensors' will record, successively, the *P/T* and the *S/T* waves. The maximum pressure of both the *P/T* and *S/T* converted waves generated by double-couple mechanisms are observed at notable angles around 80° with respect to the vertical (Figs 3b and c). These phases will thus be efficiently trapped and guided by the SOFAR, a process that requires low enough grazing angles (Williams *et al.* 2006). Moreover, our model shows that the contribution of the *S/T* converted waves exceeds that of the *P/T* converted wave for most offset angles. Finally, the orientation of the double-couple mechanism (i.e. its angle versus the vertical in our 2-D modelling scheme) influences the relative contributions of the *P/T* and *S/T* waves to the acoustic signal.

5 CONCLUSIONS

We have developed the SOLFLU code to achieve a direct model of the seismic to acoustic conversion of waves across the seafloor interface, by solving the fundamental equations of continuum mechanics. This code models the conversion of the waves generated by two different source mechanisms: a purely explosive source and a double-couple one. Our work provides two main results. First, water-column *T* waves can be generated by shallow crust double-couple mechanisms and enter the SOFAR channel with efficient incidence angles, thus allowing them to be trapped and propagate in the waveguide. Such *T* waves can be produced without the presence of a regional sloped topography, thus, overcoming the '*T*-phase paradox' and without any local specific roughness characteristics of the seafloor. Second, our model confirms the results of the modal propagation model (Park *et al.* 2001), that is, that *S* waves are more efficient than *P* waves in producing energetic *T* waves.

Our results therefore bear direct consequences on the way earthquake size estimates can be derived from hydrophone source level observations. We show that sources that have a higher relative *S*-wave content are likely to produce higher-SL acoustic signals, for earthquakes with equal magnitudes. Therefore, empirical studies that develop relationships between acoustic source level and earthquake magnitude need to take source mechanism, and therefore *S*-wave radiation patterns, into account. A study by Dziak (2001) found that two distinct magnitude/SL empirical linear relations, based on the source earthquake fault orientation, were necessary to properly describe the seismic to acoustic energy distribution of 179 seismic NE Pacific earthquakes. Dziak proposed that *T*-phase energy at the seafloor–ocean interface would be lower for normal/reverse faults than for strike-slip events, an effect which he attributed to the *S*-wave radiation pattern, which would be different between the fault types. Strike-slip events produce *S*-wave energy with horizontal particle motion (parallel to seafloor ocean interface).

We are currently working to model the conversion in a more realistic context. In particular, a more complex first-order regional seafloor topography will be input in the model. Implementing a more realistic topography requires a precise choice of the grid element size to ensure that running the model will not exceed 'reasonable' computer resources. Extension of the SOLFLU code to 3-D is also envisioned to obtain a realistic view of the propagation wave-field. Finally, we plan to use the ouputs of our model as inputs in acoustic propagation models to compute the effects of long-distance paths in the SOFAR channel. When these steps are completed, it will be possible to invert *T*-phase waveforms recorded by hydrophone arrays directly to derive earthquake seismic magnitudes.

ACKNOWLEDGMENTS

We wish to thank Edouard Canot (IRISA, Rennes) for having provided to us the initial FLUSOL code, which was used as a base for the development of SOLFLU. We also thank Bob Dziak and Bob Odom for fruitfull discussions on many intriguing questions *T* waves keep concealing.

REFERENCES

Bécache, E., Joly, P. & Tsogka, C., 2001. Application of the fictitious domain method to 2D linear elatodynamic problems, *J. Comput. Acoust.,* **9,** 1175–1202.

Collino, F. & Tsogka, C., 2001. Application of the pml absorbing layer model to the linear elastodynamic problem in anisotropic heterogeneous media, *Geophysics,* **66,** 294–307.

de Groot-Hedlin, C.D. & Orcutt, J.A., 1999. Synthesis of earthquake-generated *T*-waves, *Geophys. Res. Lett.,* **26,** 1227–1230.

Dziak, R., 2001. Empirical relationship of *T*-wave energy and fault parameters of Norheast Pacific ocean earthquakes, *Geophys. Res. Lett.,* **28,** 2537–2540.

Dziak, R. et al., 2004. *P*- and *T*-wave detection thresholds, *Pn* velocity estimate, and detection of lower mantle and core *P*-waves on ocean sound-channel hydrophones at the mid-atlantic ridge, *Bull. seism. Soc. Am.,* **95,** 665–677.

Fox, C. & Dziak, R., 1999. Internal deformation of the gorda plate observed by hydroacoustic monitoring, *J. geophys. Res.,* **106,** 17 603–17 615.

Fox, C., Matsumoto, H. & Lau, T.-K., 2001. Monitoring pacific ocean seismicity from an autonomous hydrophone array, *J. geophys. Res.,* **106,** 4183–4206.

Goslin, J., Lourenço, N., Dziak, R.P., Bohnenstiehl, D.R., Haxel, J. & Luis, J., 2005. Long-term seismicity of the Reykjanes Ridge (North Atlantic) recorded by a regional hydrophone array, *Geophys. J. Int.,* **162,** 516–524.

Johnson, R.H., Northrop, J. & Eppley, R., 1963. Sources of Pacific *T*-phases, *J. geophys. Res.,* **68,** 4251–4260.

Park, M., Odom, R.I. & Soukup, D.J., 2001. Modal scattering: A key to understanding oceanic *T*-waves, *Geophys. Res. Lett.,* **28,** 3401–3404.

Talandier, J. & Okal, E.A., 1998. On the mechanism of conversion of seismic waves to and from *T*-waves in the vicinity of island shores, *Bull. seism. Soc. Am.,* **88,** 621–632.

Williams, C.M., Stephen, R.A. & Smith, D.K., 2006. Hydroacoustic events located at the intersection of the Atlantis (30°N) and Kane (23°40′N) transform faults with the Mid-Atlantic Ridge, *Geochem. Geophys. Geosyst.,* **7,** Q06015, doi: 10.1029/2005GC001127.

Zhein, S., Canot, E., Erhel, J. & Nassif, N., 2004. Developement de nouveaux moyens d' exploration géophysique: mise au point d'un modèle numérique pour la propagation des ondes élastiques, IFREMER internal report.